JGR Space Physics

RESEARCH ARTICLE
10.1029/2024JA032971

Reproducing Ultra-Relativistic Electron Acceleration Using a Coupled Density and Radiation Belt Model

T. A. Daggitt[1,2], R. B. Horne[1], S. A. Glauert[1], and G. Del Zanna[2]

[1]British Antarctic Survey, Cambridge, UK, [2]Department of Applied Mathematics and Theoretical Physics, University of Cambridge, Cambridge, UK

Key Points:

- More realistic information about the plasma density leads to better recreations of multi-MeV electron flux enhancements in a diffusion model
- Chorus waves can directly accelerate electrons to multi-MeV energies at L* = 4 when the plasma density is low, without radial diffusion
- The Van Allen Probes f_{pe}/f_{ce} measurements are biased away from values less than 2.5

Supporting Information:

Supporting Information may be found in the online version of this article.

Correspondence to:

T. A. Daggitt,
thoggi18@bas.ac.uk

Citation:

Daggitt, T. A., Horne, R. B., Glauert, S. A., & Del Zanna, G. (2024). Reproducing ultra-relativistic electron acceleration using a coupled density and radiation belt model. *Journal of Geophysical Research: Space Physics*, *129*, e2024JA032971. https://doi.org/10.1029/2024JA032971

Received 14 JUN 2024
Accepted 2 DEC 2024

Author Contributions:

Conceptualization: T. A. Daggitt, R. B. Horne, S. A. Glauert, G. Del Zanna
Formal analysis: T. A. Daggitt
Methodology: T. A. Daggitt, R. B. Horne, S. A. Glauert
Software: T. A. Daggitt, S. A. Glauert
Supervision: R. B. Horne, S. A. Glauert, G. Del Zanna
Visualization: T. A. Daggitt
Writing – original draft: T. A. Daggitt
Writing – review & editing: R. B. Horne, S. A. Glauert, G. Del Zanna

Abstract The cold plasma density can significantly alter the rate of diffusion of radiation belt electrons by chorus waves within the magnetosphere, and the range of energies at which diffusion is effective. We describe a coupled density and radiation belt model based on the British Antarctic Survey Radiation Belt Model that uses spatially and temporally varying values of f_{pe}/f_{ce} to drive a statistical model of electron diffusion due to chorus waves. We demonstrate that this approach of including the variance in f_{pe}/f_{ce} recreates the acceleration of electrons up to MeV energies better than other previous approaches to including f_{pe}/f_{ce}.

Plain Language Summary The density of low energy charged particles trapped in Earth's magnetic field can influence how higher energy trapped electrons are affected by natural radio waves within the magnetic field. We describe a modification of the British Antarctic Survey Radiation Belt Model that includes a model of density that varies in both time and space. These density values are used to drive a statistical model of electron scattering due to chorus waves. We demonstrate that including the variance of density in the model recreates the acceleration of electrons up to ultra-relativistic energies better than other previous approaches to accounting for the low energy charged particle density.

1. Introduction

Early models of the radiation belts treated the equilibrium electron flux as a balance between acceleration by inwards radial diffusion and loss due to pitch angle scattering (Haerendel, 1970). Lyons and Thorne (1973) showed that this approach could accurately reproduce equilibrium electron flux distributions up to energies of 2 MeV, but underestimated higher energy fluxes. Two main theories are commonly used to explain this additional acceleration of multi-MeV electrons, enhanced radial diffusion driven by ULF waves (Mathie & Mann, 2000; Rostoker et al., 1998), or local acceleration driven by wave-particle interactions between electrons and chorus waves (Horne & Thorne, 1998; Summers et al., 1998).

Horne et al. (2005) showed observations of strong chorus waves at a range of L^* observed at Antarctic ground stations and the Cluster spacecraft. They demonstrated that diffusion coefficients from the observed wave power distribution could increase the flux of 1 MeV electrons by multiple orders of magnitude in a 1D energy diffusion simulation including loss timescales. They also showed that the rate of enhancement depended heavily on the cold plasma density. More recent studies of multi-MeV electron enhancements have used observations from the Van Allen Probes (VAP) mission in 2012, referring to the ultra-relativistic (≥2 MeV) population (Shprits et al., 2022; Zhao et al., 2019). Allison and Shprits (2020) analyzed contours of electron phase-space density observed by the VAP satellites, demonstrating that local acceleration by chorus waves was capable of accelerating electrons directly up to 7 MeV.

Allison et al. (2021) showed that reducing the background cold plasma density could increase the rate of energy diffusion due to chorus waves at high energies, and that these coefficients could effectively accelerate electrons up to 7 MeV in a 2D simulation without radial diffusion. Shprits et al. (2022) compared observations of ultra-relativistic enhancements with the cold plasma density over 4.5 years of VAP data, showing a clear association between density depletions and enhancements. The cold plasma density can affect the resonant energies at which interactions between whistler mode waves and electrons efficiently accelerate electrons (Glauert & Horne, 2005; Horne & Thorne, 1998).

In addition to the effect of low cold plasma density on wave-particle interactions, the distribution of chorus waves has been shown to depend on the cold plasma density. D. Hartley et al. (2023) and Wong et al. (2024) observed

two distinct distributions of chorus wave normal angles in statistical studies of chorus waves at different densities. The growth rate of chorus waves at different densities also depends on the cold plasma density, leading to enhanced or suppressed chorus wave activity at different frequencies (He et al., 2022; Tang et al., 2014).

Most previous work simulating the radiation belts have captured the effects of the cold plasma density by averaging over it, either before or after calculating diffusion coefficients (Glauert et al., 2014a; Kersten et al., 2014; Ross et al., 2020; Subbotin & Shprits, 2009). Although there has been some work put into simulating the radiation belts using the cold plasma density as a driving parameter (Allison et al., 2021; Guo et al., 2023), these studies have either not attempted to recreate the full radiation belts, or have used event specific chorus waves.

In this paper we present the first use of a coupled density and radiation belt model. We use this model together with a density-driven statistical chorus model to investigate the effects of time-varying cold-plasma density on the recreation of ultra-relativistic electron flux during a geomagnetic storm by the British Antarctic Survey Radiation Belt Model (BAS-RBM).

2. Data and Methodology

2.1. Dependence of Diffusion Coefficients on f_{pe}/f_{ce}

The background cold plasma density alters the electron plasma frequency, f_{pe}, the frequency of electrostatic oscillations of electrons in a cold plasma. For a cold plasma, where thermal motion is ignored, f_{pe} is given by

$$f_{pe} = \frac{1}{2\pi}\sqrt{\frac{n_e q^2}{\epsilon_0 m_e}} \tag{1}$$

where n_e is the electron number density, e is the electron charge, m_e is the electron rest mass and ϵ_0 is the vacuum permittivity. The effect of the cold plasma density on wave-particle interactions is usually parameterized by the ratio of f_{pe} to the electron gyrofrequency, f_{ce}, expressed as f_{pe}/f_{ce}, related to the plasma refractive index. The expression for f_{pe}/f_{ce} in a cold plasma in magnetic field of magnitude B is

$$\frac{f_{pe}}{f_{ce}} = \sqrt{\frac{n_e m_e}{\epsilon_0 B^2}} \tag{2}$$

f_{pe}/f_{ce} is an important parameter for modeling wave-particle interactions in a cold plasma, as it alters the minimum resonant energy. This is because the wave phase speed is dependent on f_{pe}/f_{ce}, which in turn affects the lowest value of $v_{\|}$, the field aligned component of the electron velocity, for which an electron of a given energy can interact with a circularly polarized plasma wave via Doppler-shifted cyclotron resonance (Summers & Thorne, 2003). As f_{pe}/f_{ce} decreases, the minimum resonant energy increases, and the diffusion rate increases for high energy electrons.

Figure 1 shows the effect of reducing f_{pe}/f_{ce} on diffusion coefficients calculated for a sample wave distribution. This figure shows that both acceleration and pitch angle scattering of electrons due to chorus waves becomes significantly more efficient as f_{pe}/f_{ce} drops closer to one. This will result in both more rapid loss and more rapid enhancements of high energy electrons. As D_{EE} increases more rapidly with decreasing f_{pe}/f_{ce} than $D_{\alpha\alpha}$ and $|D_{\alpha E}|$, this suggests that the increased acceleration can dominate over the increased losses. However, multiple other factors are at play in the radiation belts, including whether effective pitch angle diffusion extends all the way to the loss cone, and the gradient of the electron energy spectrum. Determining which of these effects dominates in practice requires full simulations of the electron phase space density distribution under realistic radiation belt conditions.

Because the rate of diffusion due to VLF wave interactions can depend heavily on the value of f_{pe}/f_{ce}, previous approaches to producing statistical models of VLF wave diffusion coefficients have used a variety of methods to account for the effect of f_{pe}/f_{ce}.

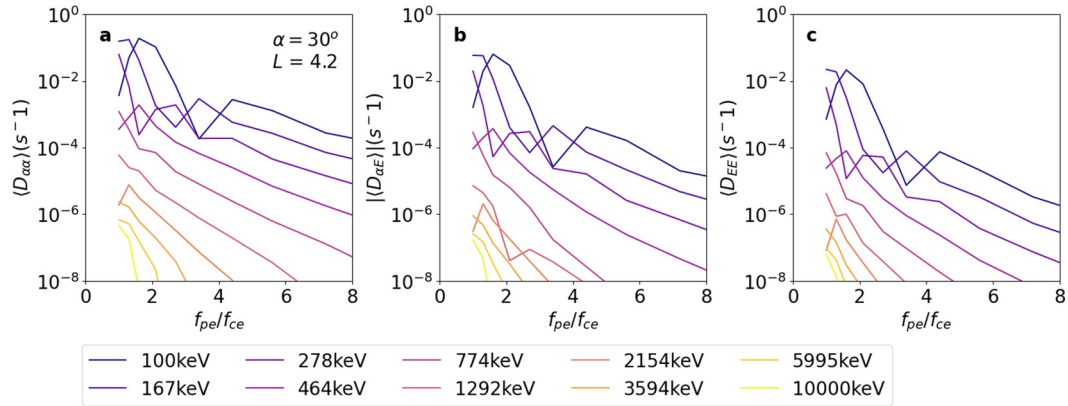

Figure 1. (a, b, c) Bounce-averaged $D_{\alpha\alpha}$, $|D_{\alpha E}|$ and D_{EE} coefficients calculated using a sample chorus wave distribution at different values of f_{pe}/f_{ce}, at $\alpha = 30^o$, $L = 4.2$. These coefficients were calculated using the PADIE code (Glauert & Horne, 2005), with a Gaussian distribution of frequencies, $\mu = 0.25f_{ce}$ and $\sigma = 0.05f_{ce}$. The wave normal angle distribution was centered at zero, with a width of 30^o, and the waves were assumed to be confined to MLAT $\leq 10^o$.

2.2. f_{pe}/f_{ce} Averaged Diffusion Coefficients

A simple approach is to use a model of the f_{pe}/f_{ce} value on a grid of L^* and MLT, and select f_{pe}/f_{ce} values from this model when calculating diffusion coefficients at different L^* an MLT. The f_{pe}/f_{ce} values may be additionally parameterized by geomagnetic activity to account for more of the variance in f_{pe}/f_{ce}. This approach has been used to calculate chorus (Horne et al., 2013) and hiss (Glauert et al., 2014b) diffusion coefficients based of f_{pe}/f_{ce} observations by the CRRES satellite, and EMIC diffusion coefficients based on a fixed f_{pe}/f_{ce} value (Kersten et al., 2014), and f_{pe}/f_{ce} values from an empirical plasmaspheric density model (Ma et al., 2015). Diffusion coefficients calculated using this method have been successfully used to recreate a variety of radiation belt phenomena using the BAS-RBM and other models (Glauert et al., 2014b, 2018; Ma et al., 2015; Varotsou et al., 2008). For this study, the f_{pe}/f_{ce} averaged chorus diffusion coefficients used were derived from the Meredith et al. (2020) chorus model, using activity-dependent f_{pe}/f_{ce} values from the model described in Horne et al. (2013).

2.3. Co-Located Diffusion Coefficients

Watt et al. (2019) showed that the mean of multiple diffusion coefficients calculated from simultaneous measurements of wave power and f_{pe}/f_{ce} can vary significantly compared to the single diffusion coefficient calculated from the mean wave power and mean f_{pe}/f_{ce}. Ross et al. (2020) used this co-located approach to calculate new diffusion coefficients for EMIC waves, and demonstrated that this approach resulted in better agreement between the BAS-RBM and observational data than the EMIC models of Kersten et al. (2014) and Ma et al. (2015). As it is highly computationally expensive to calculate diffusion coefficients for every observation and then average them, Ross et al. (2021) further developed this method by approximating the full co-located calculation. Each EMIC wave observation was binned by f_{pe}/f_{ce}, location and activity, bounce-averaged diffusion coefficients were then calculated for each f_{pe}/f_{ce} bin and then added together, weighted by the number of observations in each f_{pe}/f_{ce} bin. This method showed close agreement with the values of the bounce-averaged diffusion coefficients given by the full calculation. Wong et al. (2024) recently used the method of Ross et al. (2021) to calculate approximated co-located chorus diffusion coefficients using the statistical wave model of Meredith et al. (2020) and observations from the entire VAP mission. These coefficients have been compared to previous chorus diffusion models, but have not yet been used to drive a radiation belt model. This study uses the Wong et al. (2024) chorus model as an example of co-located chorus diffusion coefficients.

2.4. Coupled-Density Diffusion Coefficients

To produce the chorus diffusion model in Wong et al. (2024), the authors binned each measurement of the wave and plasma properties by f_{pe}/f_{ce}, calculated diffusion coefficients across the model domain for each f_{pe}/f_{ce} bin, and then averaged over f_{pe}/f_{ce} for the final result, weighting by the number of observations in each f_{pe}/f_{ce} bin. Of

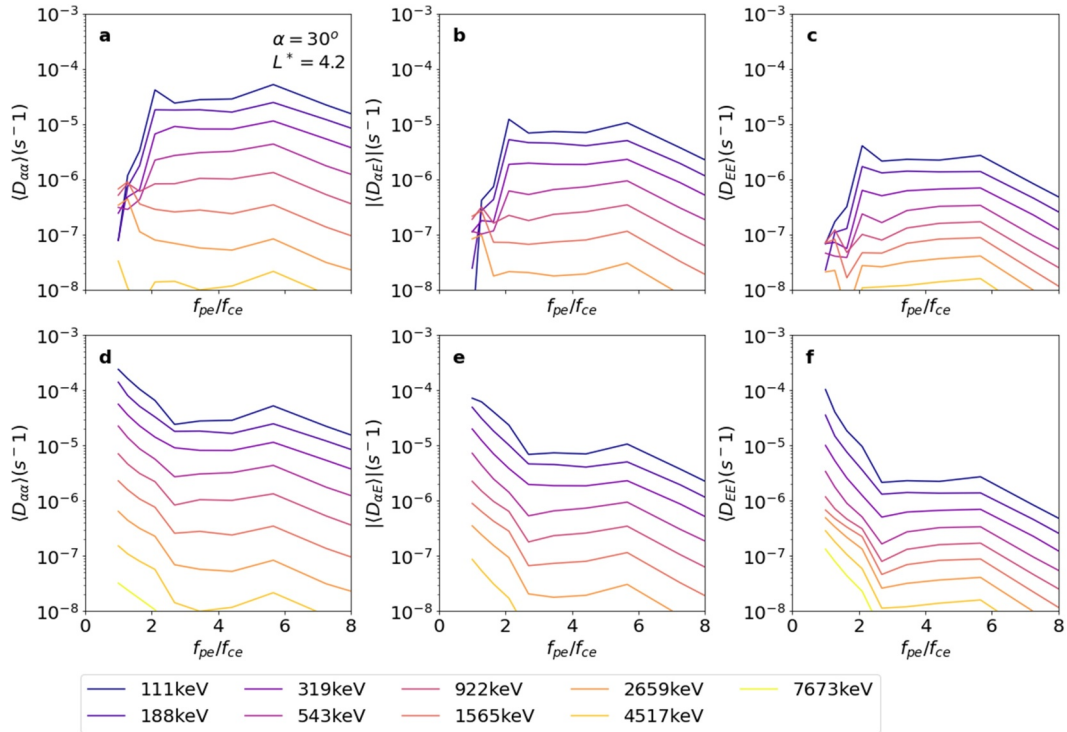

Figure 2. (a, b, c) Bounce- and drift-averaged $D_{\alpha\alpha}$, $|D_{\alpha E}|$ and D_{EE} values from the Wong et al. (2024) chorus model versus. f_{pe}/f_{ce} at Kp = 4, $\alpha = 30^o$, $L^* = 4.2$. (d, e, f) The same coefficients in (a, b, c) with the correction defined in Section 2.4 applied at low f_{pe}/f_{ce}.

particular interest are the intermediate values from before the final weighted average. These values allow for a third approach to characterizing the effects of f_{pe}/f_{ce} on the behavior of the radiation belts. With individual diffusion coefficients at different f_{pe}/f_{ce} values, it is possible to couple a model of the background plasma density to the BAS-RBM, and use it to select diffusion coefficients at different f_{pe}/f_{ce} values.

The f_{pe}/f_{ce} binned bounce- and drift-averaged diffusion coefficients of Wong et al. (2024) for $f_{pe}/f_{ce} < 8$ are shown in Figures 2a–2c. Whilst the diffusion coefficients for some energies in 2a–c increase below $f_{pe}/f_{ce} = 2$, most of them, especially below 1 MeV, drop off significantly as f_{pe}/f_{ce} approaches one. This is unexpected as local diffusion coefficients tend to increase as f_{pe}/f_{ce} decreases (Allison et al., 2021; Glauert & Horne, 2005), as shown in Figure 1. The authors do not include these low f_{pe}/f_{ce} bins in the calculation of the final co-located chorus model as the number of VAP observations in these bins is below 100, the cut-off they chose for sufficient statistical strength. In order to extend the coupled-density chorus diffusion model to lower f_{pe}/f_{ce}, where the rate of diffusion is expected to be highest, a correction to the diffusion coefficients below $f_{pe}/f_{ce} = 2.5$ is required. Following Wong et al. (2024), the existing diffusion coefficients in these bins are not trusted due to the low statistical power of the small number of wave observations in these bins. The approach used for these corrections was to recalculate the binned chorus wave and plasma parameters in the $2.1 < f_{pe}/f_{ce} < 2.7$ bin using binning method described in Wong et al. (2024). The wave and plasma parameters used were the plasma density, dipole L value, the latitude range over which waves were observed, wave normal angle distribution, the power spectral density over a given frequency range, and relative abundances of H^+, He^+ and O^+ ions. To fill in the lower f_{pe}/f_{ce} values, each of these parameters were held constant apart from the plasma density, which was altered to produce the correct f_{pe}/f_{ce} at each L. The low number of observations from the VAP data set in these f_{pe}/f_{ce} bins means that the VAP data set does not give reliable information on the distributions of wave and plasma parameters in this region. In the absence of other cross-calibrated data sets of chorus wave and plasma parameter observations in this regime, constant parameters were used as a conservative assumption. In reality, the chorus wave power may vary at low densities as the growth rate of chorus is dependent on the cold plasma density, leading to enhanced or suppressed

chorus wave activity at different frequencies (He et al., 2022; Tang et al., 2014). Diffusion coefficients for each of the lower f_{pe}/f_{ce} bins were recalculated using the PADIE code (Glauert & Horne, 2005) with these fixed chorus wave and plasma parameters. Further details on the method for producing bounce- and drift-averaged chorus diffusion coefficients from the chorus wave and plasma parameters can be found in Wong et al. (2024). The results of this correction are shown in Figures 2d–2f, demonstrating increased diffusion coefficients below $f_{pe}/f_{ce} = 2.5$. As the corrected diffusion coefficients will result in both more pitch angle and energy diffusion, the corrected diffusion model will result in both more local acceleration of electrons, and more loss due to pitch angle diffusion into the loss cone, it is not clear which of these effects will dominate without simulation. The motivation for this correction is discussed further in Section 4. This corrected chorus model can then be used in conjunction with a plasmaspheric density model to investigate the effects of time-varying f_{pe}/f_{ce} on the acceleration of electrons by chorus waves.

The advantage of using co-located diffusion coefficients over the averaged diffusion coefficients is that the co-located diffusion coefficients contain contributions from the entire observed scope of wave-particle interactions. The averaged diffusion model assumes that the diffusion coefficient under average conditions is representative of the full distribution of diffusion coefficients over all observed wave and plasma parameters. Watt et al. (2019) showed that the distributions of diffusion coefficients calculated for each simultaneous measurement of wave power and f_{pe}/f_{ce} are non-Gaussian, and that the distributions vary with L and geomagnetic activity. The co-located diffusion coefficients capture more of the range of possible wave and plasma parameters, as well as the variability in their distributions across L and geomagnetic activity, and have been shown to improve the recreation of observational data (Ross et al., 2020). The coupled-density diffusion model is expected to improve on the co-located diffusion model for similar reasons. By removing the averaging over f_{pe}/f_{ce}, the extremes of the range of observed wave and plasma parameters are better captured in the model. This will have the largest effect during geomagnetic storms, when the most extreme conditions are observed. The averaged and co-located diffusion models attempt to capture the change in conditions during storms by binning by geomagnetic activity, but there is inevitably some spread in the wave and plasma parameters within each geomagnetic activity bin as they are not perfectly correlated with activity. By binning the observations by an additional parameter, f_{pe}/f_{ce}, the distribution of wave parameters averaged over within each bin to produce diffusion coefficients should be narrower. This is because any variation of f_{pe}/f_{ce} within each larger bin has been removed. This improves the representation of extreme conditions that would otherwise be averaged with a low weight into a more general diffusion coefficient.

The co-located chorus diffusion model and the coupled-density chorus diffusion model both require the same number of diffusion coefficient calculations. The difference between the two is that in the co-located model, the bounce- and drift-averaged diffusion coefficients calculated for each f_{pe}/f_{ce} bin are averaged together, weighted by the number of observations in each f_{pe}/f_{ce} bin, resulting in a 4 dimensional model (geomagnetic activity, electron equatorial pitch angle, energy and L). This step is not performed in the coupled-density model, resulting in a 5 dimensional model with f_{pe}/f_{ce} as the additional dimension. As a result of this, time series of the geomagnetic activity and the drift-averaged density at each L shell can be used to select diffusion coefficients from the coupled-density model that vary with both the activity level and the background plasma density.

2.5. Density Model

In order to use the coupled-density diffusion coefficients in the BAS-RBM, a time series of f_{pe}/f_{ce} values must be used as an additional driving parameter for the simulation. Ideally the f_{pe}/f_{ce} time series should reproduce the variation in plasma density across the model domain, in this case varying in both L^* and time. The Carpenter & Anderson, 1992 plasmasphere model was chosen as the basis of the plasma density timeseries for this study (Carpenter & Anderson, 1992). This model was chosen for it's simple driving parameters, Kp and the monthly average sunspot number, as well as being valid from $2 < L < 8$, thus covering the normal operating range of the BAS-RBM. f_{pe}/f_{ce} values can be generated from the Carpenter and Anderson plasma density output assuming a dipole field, using Equation 2. Notably for driving the coupled-density chorus model, the f_{pe}/f_{ce} values from the Carpenter and Anderson model are mostly constrained to stay above $f_{pe}/f_{ce} = 2$. The Carpenter and Anderson plasma trough density for the lowest density MLT sector is given by Carpenter and Anderson (1992)

$$n_e = (5800 + 300t)L^{-4.5} + 1 - \exp\left(\frac{L-2}{10}\right) \quad 00 \le t < 06\ \text{MLT} \tag{3}$$

where t is the MLT in hours. Using Equation 2, this results in a minimum possible f_{pe}/f_{ce} of 2.2 at $L = 4$. The model is also limited by the time resolution of Kp, which is reported in 3 hr intervals (Matzka et al., 2021).

In order to better capture the extent of f_{pe}/f_{ce} variation and the shorter timescales that it varies over, a model was developed that used VAP-A observations from the L4 data product from the EMFISIS instrument (Kurth et al., 2015) to tune the output of the Carpenter and Anderson model. The model was generated using the following process:

1. Determine the density profile in L for the saturated plasmasphere and the plasma trough using definitions given in Carpenter and Anderson (1992).
2. Use the most recent observation of the plasmapause by VAP-A as the cut-off between the plasmasphere and plasma trough profiles, as determined using the plasmapause identification method from Wong et al. (2024).
3. Scale the plasmasphere/plasma trough density profile to match the current f_{pe}/f_{ce} measurement from VAP-A, depending on whether VAP-A is inside/outside the plasmapause.

As the BAS-RBM simulates drift-averaged electron flux, for driving the BAS-RBM the output of the fitted model is averaged over MLT to produce a single drift-averaged f_{pe}/f_{ce} profile in L. The results of this are shown for a geomagnetic storm in October 2014 in Figure 3, with the VAP-A data-driven plasmapause position from Wong et al. (2024) superimposed. Figure 3a shows that there is a gap in the VAP-A density observations between 23rd October 12:00UTC and 24th October 18:00UTC. When there is no density data available, the model uses the unaltered density values from the Carpenter and Anderson model. This results in the region of Figure 3b where the density is nearly constant in time, as the Carpenter and Anderson density varies much more slowly than the density observed by VAP-A. In combination with the coupled-density chorus diffusion coefficients, this model of f_{pe}/f_{ce} can be used to drive the BAS-RBM in order to capture the effect of time-varying f_{pe}/f_{ce} on the electron population in the outer radiation belt. The f_{pe}/f_{ce} value at each L value and time step from the density model is used to select chorus diffusion coefficients from the 16 logarithmically spaced f_{pe}/f_{ce} bins of the chorus diffusion model for each point on the BAS-RBM model grid.

2.6. The British Antarctic Survey Radiation Belt Model

3D simulations of the radiations belts were performed using the BAS-RBM (Glauert et al., 2014a, 2014b), which simulates the time-evolution of the phase-averaged electron phase space density by numerically solving the Fokker-Planck equation. For the simulations in this study background corrected electron flux from the VAP MagEIS and REPT instruments (Baker et al., 2013; Blake et al., 2014; Claudepierre et al., 2015) were used for the initial condition and $L_{\min}$ boundary. The $L_{\max}$ and $E_{\min}$ boundaries were derived from GOES-15 EPEAD and MAGED data using a method similar to the method described by Glauert et al. (2018), with minor modifications. The integral and differential flux measurements from GOES-15 are fitted to a power law and an exponential function. The function that provides a better fit is then used to calculate the phase space density at all energies on grid at $L_{\max}$. As the satellites vary in L^* over time, the phase space density is mapped adiabatically to a fixed $L_{\max}$. The $E_{\min}$ boundary is determined using the average phase space density profile in L^* from CRRES observations at $\mu = 100$ MeV/G, $J = 0$ keV (Glauert et al., 2014a). This profile is scaled consistently at all L^* to match the phase space density at 90^o at $E_{\min}$, $L_{\max}$ on the outer boundary. The L^* values for the GOES and VAP satellites were calculated using the TS04 magnetic field model (Tsyganenko & Sitnov, 2005). The BAS-RBM assumes a dipole magnetic field, and thus $L = L^*$.

3. Event Simulation

The previous work simulating the effects of hiss and chorus waves on the electron population in the outer radiation belt using the BAS-RBM has only used the first, averaged approach to including the effects of f_{pe}/f_{ce} discussed in Section 2.1 (Glauert et al., 2014a, 2018). The effects of EMIC waves have been investigated in the BAS-RBM using both the average and co-located approach to including f_{pe}/f_{ce} (Kersten et al., 2014; Ross et al., 2020). In order to test the effects of using all three approaches with chorus waves an enhancement of the

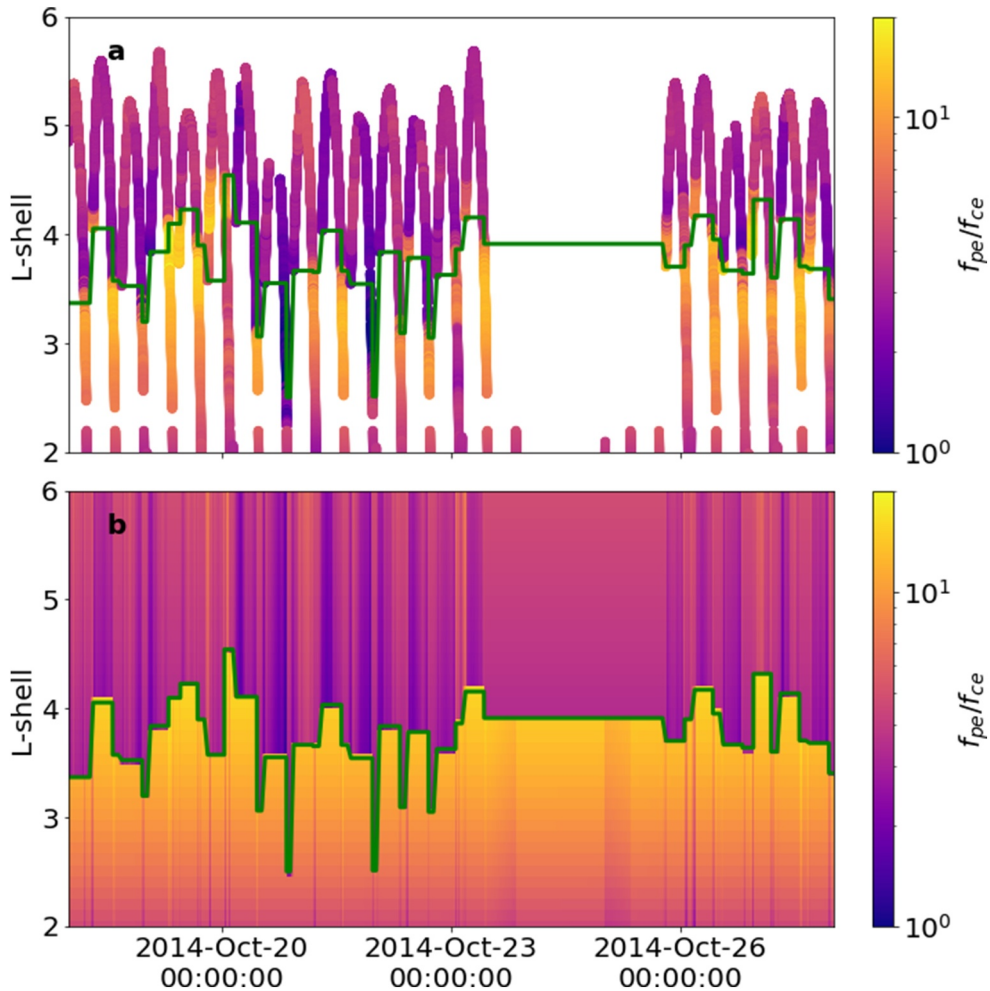

Figure 3. (a) f_{pe}/f_{ce} data from the VAP-A L4 data set, the plasmapause position is shown by the green line. (b). The f_{pe}/f_{ce} values calculated from the drift-averaged density generated by fitting the Carpenter and Anderson model to VAP-A observations as described in Section 2.5.

ultra-relativistic electron population observed by the VAP satellites from 18 to 28 October was simulated using the BAS-RBM with three different chorus diffusion models. These models were the averaged f_{pe}/f_{ce} model based on the Meredith et al. (2020) chorus model, the co-located chorus model from Wong et al. (2024), and the coupled f_{pe}/f_{ce} chorus model derived from Wong et al. (2024). The effects of EMIC waves, hiss and lightning generated whistlers were also included using statistical wave models driven by the Kp index (Glauert et al., 2014a; Ross et al., 2020).

The effects of radial diffusion are included using the electric D_{LL} coefficients from Liu et al. (2016) and the magnetic D_{LL} coefficients from Ali et al. (2016), following the method of Guo et al. (2023), referred to as the Liu and Ali radial diffusion coefficients. These radial diffusion coefficients are used as they are energy dependent, unlike the diffusion coefficients of Brautigam and Albert (2000), which have been demonstrated to overestimate the effect of radial diffusion at MeV energies and lower L^* (Guo et al., 2023).

Figure 4 shows the results of three BAS-RBM simulations using these three different chorus models, and a comparison to VAP-A and B data at 2.2 MeV and $\alpha = 85^o$. At $L^* = 3.5$ (Figure 4e) all three simulation overestimate the 2.2 MeV electron flux, showing gradual enhancement of the electron flux over the course of the event, rather than the initial decrease in flux shown in the VAP data. The difference between the three chorus models becomes more apparent at higher L^*. At $L^* = 4.3$ (Figure 4f) the coupled-density chorus model (yellow line) results in two orders of magnitude higher electron flux at 2.2 MeV than the averaged f_{pe}/f_{ce} chorus model

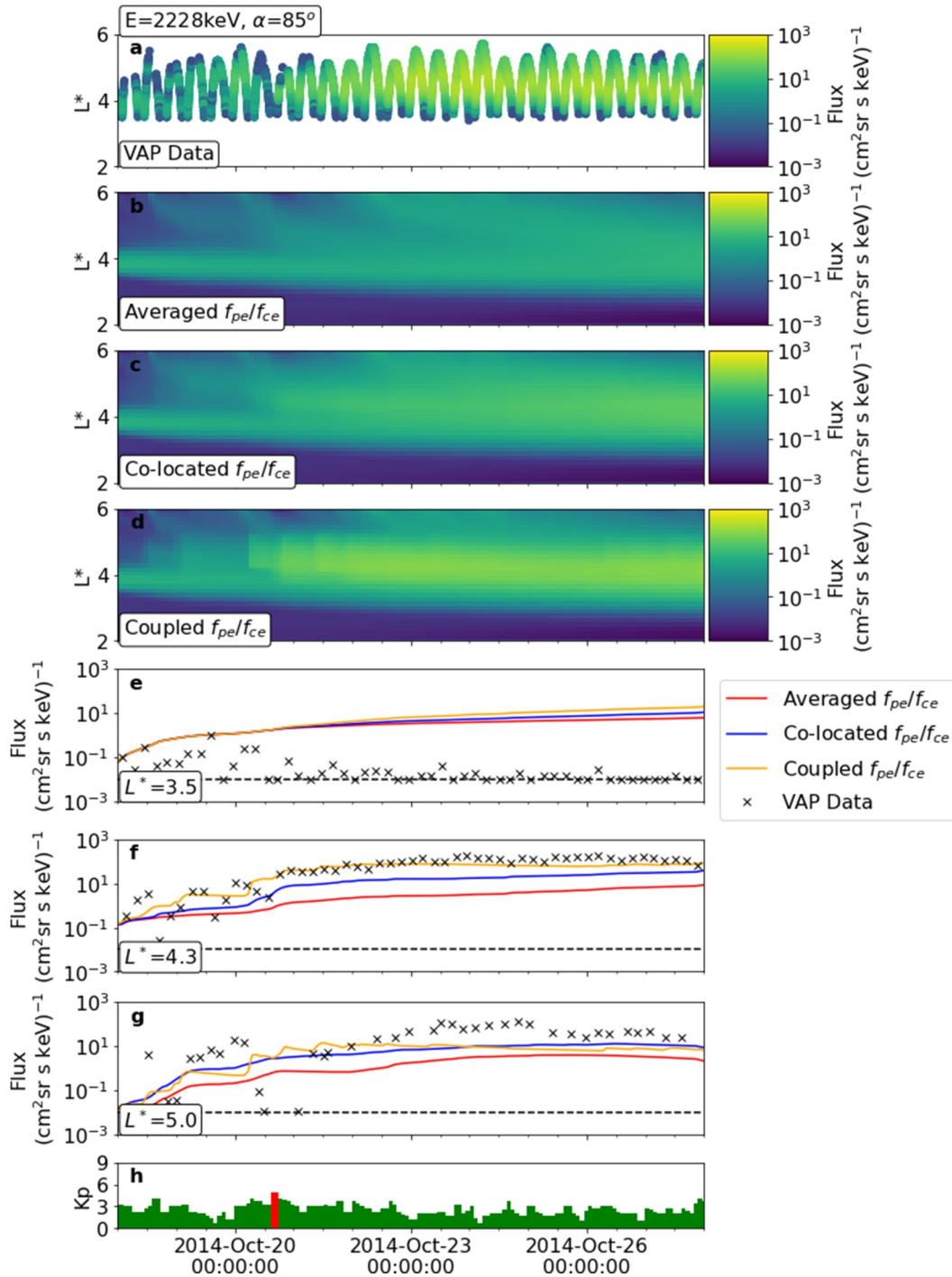

Figure 4. Summary of BAS-RBM simulations of the October 2014 event, showing differential electron fluxes at 2.2 MeV. (a) Data from the VAP-A and B MAGEIS instrument. (b) BAS-RBM electron flux from a simulation with chorus diffusion coefficients calculated using the average f_{pe}/f_{ce} value in each observation bin. (c) BAS-RBM electron flux from a simulation with chorus diffusion coefficients calculated using co-located measurements of f_{pe}/f_{ce} and chorus wave power. (d) BAS-RBM electron flux from a simulation with chorus diffusion coefficients calculated at a range of f_{pe}/f_{ce} values, driven using the density model described in Section 2.5. (e, f, g) The electron flux from VAP-A and the BAS-RBM simulations at $L^* = 3.5$, 4.3 and 5.0. The horizontal dashed line shows the VAP noise floor. (h) The Kp index during the event.

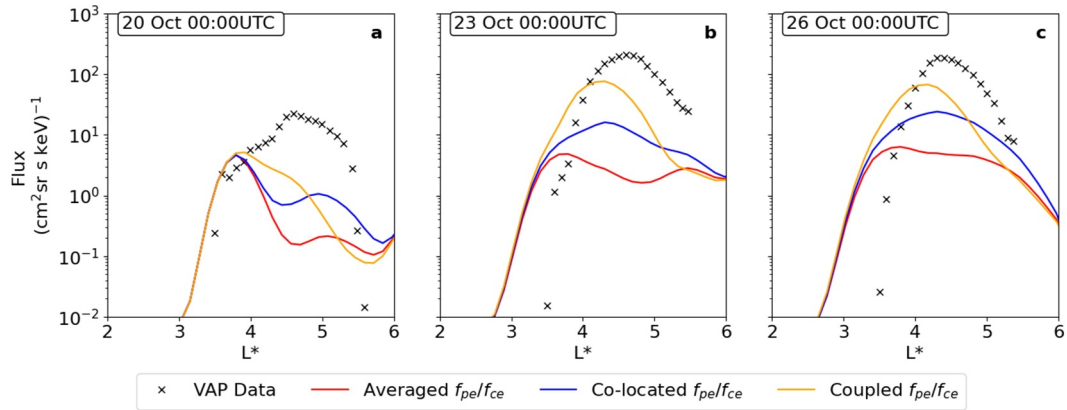

Figure 5. 2.2 MeV differential electron flux distributions in L^* at fixed points in time during the simulations shown in Figure 4.

(red line) after the electron flux begins to plateau, and one order of magnitude more than the co-located chorus model (blue line). In doing this it reproduces the VAP observations significantly better than the other two models. The co-located and coupled-density chorus diffusion models perform similarly well at $L^* = 5.0$, but still underestimate the peak electron flux. The coupled-density model also shows more rapid variations in the rate of change of electron flux than either of the other models between 20th and 23rd October, as seen in Figure 4g. These variations coincide with VAP-A observations of the plasmapause, and are likely due to rapid variation in the density model used to drive the BAS-RBM caused by the switch between fitting the plasmasphere profile and fitting the plasma trough profile to VAP-A observations.

Figure 5 shows the electron flux profiles in L^* from VAP observations and the BAS-RBM simulations at three equally spaced times during the event shown in 4. Figure 5 demonstrates that all of the BAS-RBM simulations underestimate the peak of the radial distribution of 2.2 MeV electron flux, as well as placing the peak at a lower L^* than in the VAP observations. The co-located and coupled-density chorus models increase the size of the flux peak, but still do not reach the size of the observed peak. The co-located and coupled-density chorus models also shift the location of the peak in L^* closer to the observed location later in the event, seen in Figures 5b and 5c, but do not affect the distribution below $L^* = 3.5$. Both the missing acceleration at $L^* > 4.0$ and the additional acceleration at $L^* < 3.5$ may be caused by either overestimation of the local acceleration due to chorus waves or the acceleration by inwards radial diffusion.

In order to determine the relative effect and interactions between radial diffusion and local acceleration due to chorus waves, simulations were run where either D_{LL} or $D_{\alpha\alpha}$ and D_{EE} were set to zero. This allows investigation of the contributions of both VLF waves and ULF waves to the enhancement of multi-MeV electron populations in the outer radiation belt. Figure 6 shows the output of three BAS-RBM simulations at 2.2 MeV. The effects of ULF waves are removed by imposing $D_{LL} = 0$ in the first simulation (red line), and the effects of all included VLF waves (hiss, chorus and EMIC) are removed by imposing $D_{\alpha\alpha}, D_{EE} = 0$ in the second simulation (blue line). The third simulation uses the same D_{LL}, $D_{\alpha\alpha}$ and D_{EE} values as the coupled-density simulation in Figure 6 (yellow line). The chorus model used in the first and third simulations is the coupled-density chorus model.

From Figure 6e, it is clear that the overestimation of the 2.2 MeV flux at $L^* = 3.5$ is caused by radial diffusion. Without radial diffusion (red line) the simulated flux remains mostly constant, close to the observed level. Without any VLF wave interactions, radial diffusion alone (blue line) is able to reproduce almost all the acceleration seen in the simulation with both VLF waves and radial diffusion. Comparison of the red and blue lines in Figure 6f shows that the additional acceleration from the coupled-density chorus model is primarily responsible for the enhancement in electron flux seen at $L^* = 4.3$, radial diffusion alone (blue line) is acting too slowly to reproduce the rapid acceleration seen between the 19th and 22nd of October. The comparison between the simulation without the radial diffusion (blue line) and the simulation with both radial diffusion and local acceleration (yellow line) shows that the local acceleration is responsible for nearly all of the initial acceleration. This is trend is shared by the flux at $L^* = 5.0$, where there is no visible effect of radial diffusion whilst the

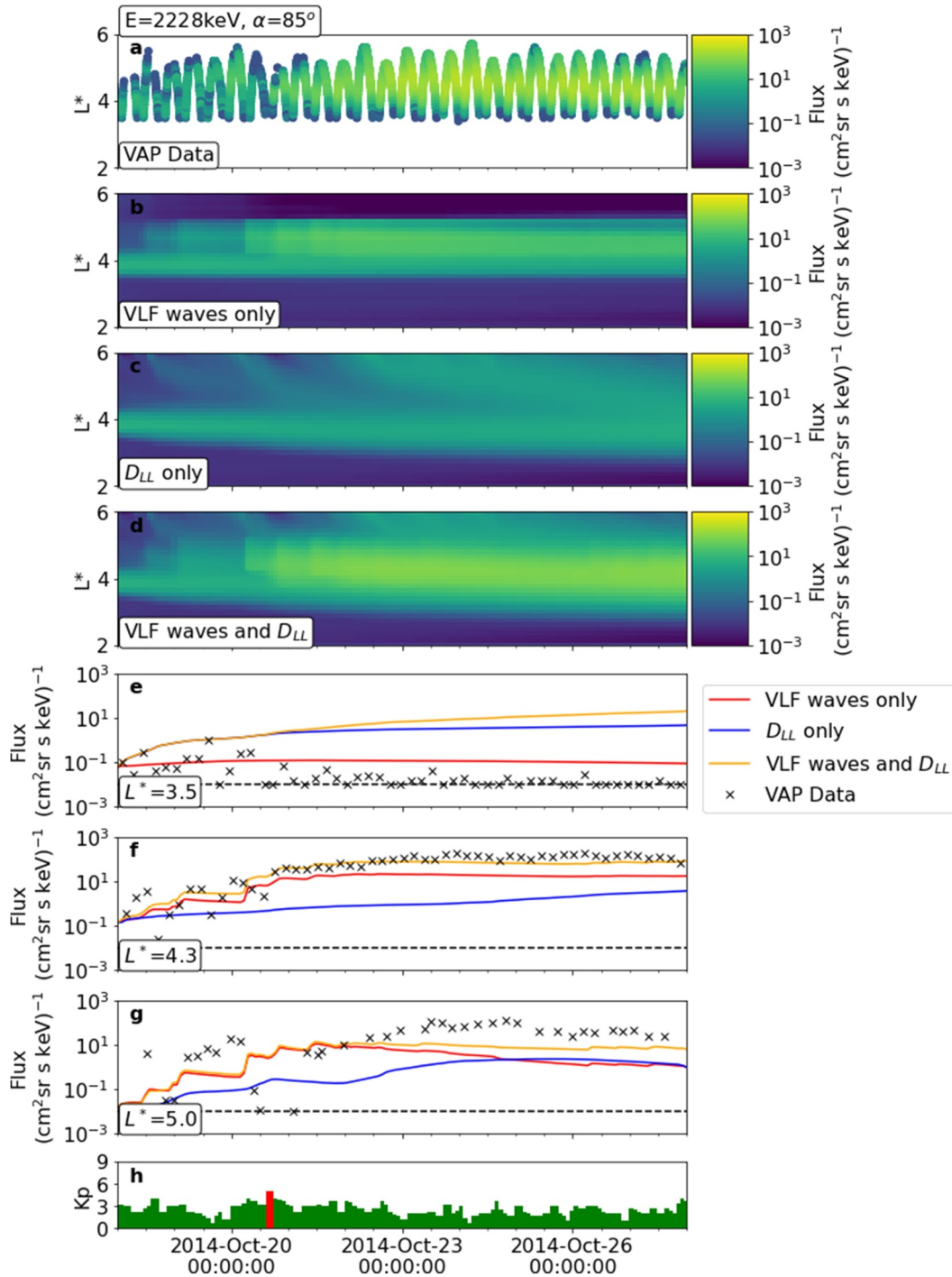

Figure 6. Summary of BAS-RBM simulations of the October 2014 event, showing differential electron fluxes at 2.2 MeV. (a) Data from the VAP-A and B MAGEIS instrument. (b) BAS-RBM electron flux from a simulation with $D_{LL} = 0$. (c) BAS-RBM electron flux from a simulation with $D_{\alpha\alpha}$, $D_{EE} = 0$. (d) BAS-RBM electron flux from a simulation with $D_{\alpha\alpha}$ and D_{EE} from VLF wave models, and D_{LL} from the combined Liu and Ali model. (e, f, g) The electron flux from VAP-A and the BAS-RBM simulations at $L^* = 3.5$, 4.3 and 5.0. The horizontal dashed line shows the VAP noise floor. (h) The Kp index during the event.

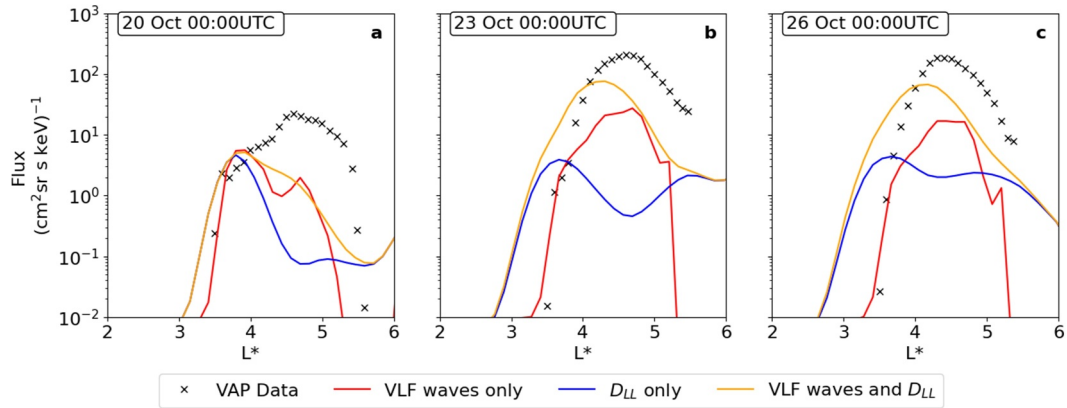

Figure 7. 2.2 MeV differential electron flux distributions in L^* at fixed points in time during the simulations shown in Figure 6.

simulated flux is still rising. It is only after the flux in the VLF waves only simulation begins to decline that the effect of radial diffusion becomes visible.

Figure 7 demonstrates that the overestimation at $L^* < 3.5$ seen in Figure 5 is due to inwards radial diffusion, as the simulation with only VLF waves (red line) closely matches the observed flux in this region. In the other two simulations, radial diffusion has shifted the electron distribution to lower L^*, resulting in the overestimation. Figure 7 also shows that chorus waves are responsible for the majority of the acceleration near $L^* = 5.0$. Beyond $L^* = 5.0$, the VLF wave only simulation underestimates the observed flux as the chorus wave diffusion rate drops off significantly due to a lack of observations in this region of the chorus wave model during active times. From Figures 5 and 7 it can be seen that changing the chorus wave model has minimal effect on the electron flux below $L^* = 3.5$. This is likely because the chorus diffusion coefficients in all three models are very low in this region, as it will usually be within the plasmapause, where the chorus wave power is low (Malaspina et al., 2021; D. P. Hartley et al., 2019). The results seen in Figures 4 and 6 extend to higher energies (see Supporting Information S1).

4. Discussion

The coupled-density chorus model described in Section 2.4 required re-calculation of the diffusion coefficients for the f_{pe}/f_{ce} bins below $f_{pe}/f_{ce} = 2.5$, as the values in these bins were unexpectedly small (see Figures 2a–2c). A bias in the wave and plasma parameters that go into the calculation of the diffusion coefficients for the $f_{pe}/f_{ce} < 2$ region of the model would result in smaller than expected diffusion coefficients.

Figure 8 shows the distribution of f_{pe}/f_{ce} measurements over the entire VAP mission in blue. There is a rapid drop-off in the frequency of observations below $f_{pe}/f_{ce} = 2.5$. From this alone it is not clear whether the lack of measurements in this region is due to how rarely f_{pe}/f_{ce} values this low occur in nature, or whether there is some systematic reason why the VAP satellites do not record low f_{pe}/f_{ce} values. The orange bars in Figure 8 shows the distribution of measurements immediately preceding or following a data gap in the L4 f_{pe}/f_{ce} data. Here there is a clear peak in the f_{pe}/f_{ce} values near $f_{pe}/f_{ce} = 3$, and the frequency of f_{pe}/f_{ce} values below 2.5 is much greater than in the distribution of all the data. This suggests that data gaps occur more frequently at lower f_{pe}/f_{ce}, and thus that small f_{pe}/f_{ce} values are under-represented in the L4 data set. The orange distribution does not distinguish between missing data during normal operation of the EMFISIS instrument, and missing data due to thruster firing events, or other events that may interrupt the normal operation of the EMFISIS instrument. Excluding these gaps would likely skew the orange distribution further toward low f_{pe}/f_{ce} values. This offers a potential explanation for the lower diffusion coefficients in this region of the chorus model of Wong et al. (2024). If chorus wave power and the plasma density are correlated, and only the start and end of periods of low f_{pe}/f_{ce} are recorded, then any strong chorus wave power during those periods will not be included in the model. Since the chorus diffusion rates are directly proportional to the wave power, this would lead to lower chorus diffusion rates than would otherwise be expected.

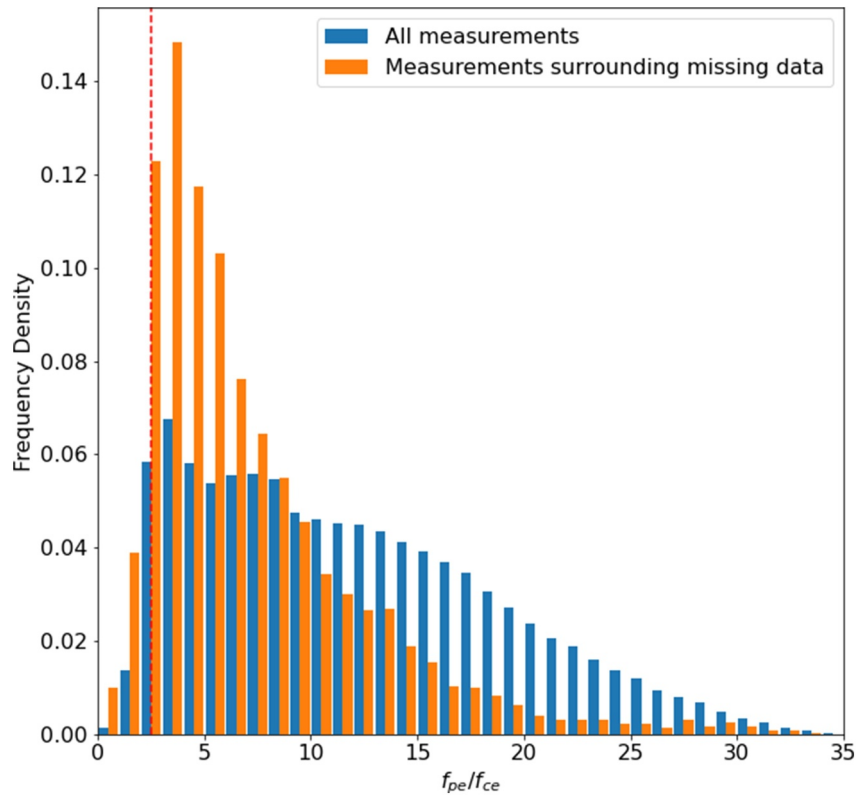

Figure 8. The distribution of f_{pe}/f_{ce} measurements from the combined VAP-A and B L4 data sets, covering the entire mission. The blue distribution contains every measurement. The orange distribution contains only measurements immediately preceding or following a gap in f_{pe}/f_{ce} data. The red dashed line shows $f_{pe}/f_{ce} = 2.5$.

The presence of gaps in the VAP density observations also leads to issues with producing density models, as seen in Figure 3a. The bias in theses gaps toward low densities will transfer to density models based on the VAP data that don't correct for the bias. The approach taken to filling the gap seen in 3a was to use density values from the un-altered Carpenter and Anderson density model. As noted in Section 2.5, the Carpenter and Anderson density model is limited in how low an f_{pe}/f_{ce} value it can produce in a dipole magnetic field. This may result in less acceleration due to chorus waves in the BAS-RBM simulations with the coupled-density chorus diffusion model, as the diffusion coefficients in the coupled-density chorus diffusion model continue to increase as f_{pe}/f_{ce} approaches 1. This is a potential cause for the underestimation of the electron flux at $L^* > 4.0$. The bias may also affect the averaged and co-located chorus diffusion models. For the averaged model, the average densities used to calculate the diffusion coefficients in each bin may be too high due to the bias. For the co-located model, the bias will result in low density diffusion coefficients being under-weighted in the averaging of the diffusion coefficients over f_{pe}/f_{ce}. Each of these effects will result in less acceleration in the averaged and co-located chorus diffusion models, and thus worse recreation of multi-MeV electrons flux enhancements.

This bias away from low f_{pe}/f_{ce} values is likely caused by the algorithm used to calculate f_{pe}/f_{ce} from observations of wave emissions near the upper hybrid resonance, f_{UHR}, used by the L4 data. Kurth et al. (2015) use f_{UHR} to determine the electron density using the relation

$$n_e = \frac{f_{UHR}^2 - f_{ce}^2}{8980^2} \tag{4}$$

The value of f_{UHR} is determined by looking at the most intense wave emission above $1.5f_{ce}$. Whilst this method can produce density measurements at high time resolution when the spectrum recorded by the EMFISIS instrument is simple, problems can occur when other wave modes are present. Kurth et al. (2015) state that electron-cyclotron harmonic emissions and diffuse electrostatic emissions can interfere with the identification. They also hesitate to

identify the $1.5f_{ce}$ band as f_{UHR} band if there are no further, weaker bands at higher frequency, or if $1.5f_{ce} <$ 10 kHz. This limits the lowest possible values of n_e that can be identified. If there is a continuum of radiation in the spectrum as opposed to distinct bands, the lower edge of the continuum is assumed to be at f_{pe}. They note that this cut-off may be due to a distant higher density structure, which would lead to overestimation of n_e and thus f_{pe}/f_{ce}. An alternative high-quality source of n_e measurements is necessary to judge the effect of the bias in this algorithm. Kurth et al. (2015) also state that during roughly 10% of VAP orbits, the f_{UHR} is difficult to identify in the outer part of the orbit, and that these times are correlated with both low densities and high geomagnetic activity. This suggests that missing density values are correlated with high chorus wave activity, which would lead to the lower diffusion rates observed in the low density part of the Wong et al. (2024) chorus model. This also suggests that the assumption made in Section 2.4 may be an underestimate of the chorus wave power, thus leading to lower acceleration in the BAS-RBM simulations using the coupled-density chorus diffusion model.

The chorus wave population at low f_{pe}/f_{ce} appears to differ significantly from the chorus wave population at higher f_{pe}/f_{ce}. With variations occurring in growth rate, wave normal angle and wave power (He et al., 2022; Tang et al., 2014; Wong et al., 2024) as f_{pe}/f_{ce} changes. Although the observations of changes in the wave normal angle and power distributions were made using the L4 data and thus share the same statistical issues as the Wong et al. (2024) chorus model at low f_{pe}/f_{ce}, it is likely that the distributions of these wave parameters continue to change as f_{pe}/f_{ce} drops toward one. Assuming that these parameters remain constant as in Section 2.4 is merely an approximation intended to work around the lack of accurate data in this regime. By resolving the bias in f_{pe}/f_{ce} observations, more accurate chorus distributions can be produced, which should improve the reproduction of ultra-relativistic enhancements by radiation belt models.

These simulations suggest that using coupled-density chorus diffusion coefficients can produce significant enhancements of multi-MeV electrons in the outer radiation belt for $L^* > 4$, resulting in up to two orders of magnitude more flux than a co-ocated or averaged f_{pe}/f_{ce} chorus model. The simulations shown in Figure 6 demonstrate that the Liu and Ali radial diffusion coefficients overestimate the rate of radial diffusion at lower L^*. They also imply that local acceleration by chorus waves is responsible for the majority of multi-MeV electron enhancement above $L^* = 4$ during this event. This is at odds with the simulations of Guo et al. (2023) which showed significant acceleration at high energies with the Liu and Ali radial diffusion coefficients alone. This discrepancy may be caused by the different boundary conditions used here. Guo et al. (2023) used VAP data at McIlwain $L = 6$ for the outer boundary, whilst the simulations here have used GOES-15 data adiabatically mapped to Roederer $L^* = 6.1$, with L^* from the TS04 magnetic field model. As a McIlwain $L = 6$ will usually correspond to an $L^* < 6$, the VAP outer boundary will be drawn from observations closer to the heart of the outer radiation belt, leading to higher flux on the outer boundary. If the electron flux on the outer boundary is already higher, then radial diffusion can appear to produce more rapid acceleration by moving that flux inwards. When the outer boundary is placed further out, additional local acceleration is required to reproduce the observations at high L^* as the flux on the outer boundary will tend to be lower.

The underestimation of the VAP electron flux by the coupled-density chorus seen in Figure 6g may be the result of the bias away from low f_{pe}/f_{ce} values in the VAP L4 data. This bias could result in missing wave power that coincides with missing density data from the statistical model of chorus wave properties, or by biasing the density model away from low f_{pe}/f_{ce} values where the acceleration of electrons by chorus waves is most efficient. Both of these effects will result in less electron acceleration by chorus waves in the BAS-RBM simulations. Correcting for the density bias, or accurately filling in gaps in the density observations result in larger chorus diffusion coefficients in averaged and co-located chorus diffusion models, and in the low-density region of the coupled-density chorus diffusion model. This would likely improve the recreation of the observed multi-MeV electron flux at $L^* > 4.0$ in the BAS-RBM.

5. Conclusions

A density-coupled statistical chorus model was developed based on the co-located chorus model of Wong et al. (2024), with a correction applied to the lowest f_{pe}/f_{ce} bins. A data-driven cold plasma density model was then developed for use with the BAS-RBM and the new density-coupled diffusion model, and compared its predictions of ultra-relativistic electron acceleration to the predictions of density-averaged and co-located chorus diffusion coefficients. The results are summarized below:

1. The use of additional information about f_{pe}/f_{ce} in the BAS-RBM leads to better recreation of ultra-relativistic electron enhancements. Co-located chorus models perform better than density-averaged chorus models, and the new coupled-density chorus model outperformed both when coupled with a data-driven density model.
2. Chorus waves at low f_{pe}/f_{ce} can recreate the majority of the enhancement of 2.2 MeV at $L^* > 4$ without radial diffusion. Radial diffusion also plays a role in the acceleration of electrons at these L^* values, but current models used with the BAS-RBM overestimate the rate of radial diffusion at lower L^*.
3. There is a bias in the VAP L4 data set away from $f_{pe}/f_{ce} < 2.5$. This bias is due to the calculation of f_{pe}/f_{ce} from emissions near f_{UHR} being less reliable during times of low plasma density. This bias likely introduced errors into the $f_{pe}/f_{ce} < 2.5$ region of the co-located chorus diffusion model of Wong et al. (2024), most of which will have been discarded before the final calculation of $D_{\alpha\alpha}$, $D_{\alpha E}$ and D_{EE}.

The majority of forecasting and simulation of the radiation belts currently uses either density-averaged or co-located diffusion models for VLF waves. This study has demonstrated that coupling the BAS-RBM to a density model can greatly improve the accuracy of the simulation, as well as demonstrating that local acceleration due to chorus waves can account for the majority of the acceleration of ultra-relativistic electrons during periods of low cold plasma density. More work is necessary to correct the issues caused by the bias in low density observations in the VAP data, this could either take the form of filling in gaps in the VAP density data, or a cross-calibrated survey of the chorus wave power that extends to lower f_{pe}/f_{ce}. The results here are focused primarily on chorus waves, but with the appropriate wave distribution, surveys could be extended to any form of VLF wave, including hiss and EMIC waves. The results are also applicable to the magnetospheres of Jupiter and Saturn, where f_{pe}/f_{ce} values close to or less than one exist for extended periods of time at high latitudes (Ma et al., 2020; Woodfield et al., 2019).

Data Availability Statement

The combined HOPE-MagEIS-REPT electron flux data from the NASA Van Allen Probes are available at https://rbsp-ect.newmexicoconsortium.org/science/DataDirectories.php (LANL, 2013). The L4 EMFISIS data from the NASA Van Allen Probes are available at https://emfisis.physics.uiowa.edu/Flight/RBSP-A/L4 (LANL, 2012). Source data are provided with this paper for the diffusion coefficients and BAS-RBM simulation data generated in this study. The files are hosted online and freely available from the NERC EDS UK Polar Data Centre database at https://doi.org/10.5285/ea37228a-5b4d-4db2-8d97-53fff2c43f3f (Daggitt et al., 2024).

Acknowledgments
This material is based upon work supported by the Air Force Office of Scientific Research under award number FA9550-19-1-7039. R. B. Horne and S. A. Glauert were also supported by the Natural Environment Research Council (NERC) grant NE/V00249X/1 (Sat-Risk) and National and Public Good activity grant NE/R016445/1. G. Del Zanna acknowledges support from STFC (UK) via the consolidated grants to the astrophysics group at DAMTP, University of Cambridge (ST/P000665/1 and ST/T000481/1).

References

Ali, A. F., Malaspina, D. M., Elkington, S. R., Jaynes, A. N., Chan, A. A., Wygant, J., & Kletzing, C. A. (2016). Electric and magnetic radial diffusion coefficients using the van Allen probes data. *Journal of Geophysical Research: Space Physics*, *121*(10), 9586–9607. https://doi.org/10.1002/2016JA023002

Allison, H. J., & Shprits, Y. Y. (2020). Local heating of radiation belt electrons to ultra-relativistic energies. *Nature Communications*, *11*(1), 4533. https://doi.org/10.1038/s41467-020-18053-z

Allison, H. J., Shprits, Y. Y., Zhelavskaya, I. S., Wang, D., & Smirnov, A. G. (2021). Gyroresonant wave-particle interactions with chorus waves during extreme depletions of plasma density in the van Allen radiation belts. *Science Advances*, *7*(5), eabc0380. https://doi.org/10.1126/sciadv.abc0380

Baker, D. N., Kanekal, S. G., Hoxie, V. C., Henderson, M. G., Li, X., Spence, H. E., et al. (2013). A long-lived relativistic electron storage ring embedded in earth's outer van Allen belt. *Science*, *340*(6129), 186–190. https://doi.org/10.1126/science.1233518

Blake, J., Carranza, P., Claudepierre, S., Clemmons, J., Crain, W., Dotan, Y., et al. (2014). *The magnetic electron ion spectrometer (MAGEIS) instruments aboard the radiation belt storm probes (RBSP) spacecraft* (pp. 383–421). The van Allen probes mission. https://doi.org/10.1007/s11214-013-9991-8

Brautigam, D., & Albert, J. (2000). Radial diffusion analysis of outer radiation belt electrons during the October 9, 1990, magnetic storm. *Journal of Geophysical Research: Space Physics*, *105*(A1), 291–309. https://doi.org/10.1029/1999JA900344

Carpenter, D., & Anderson, R. (1992). An isee/whistler model of equatorial electron density in the magnetosphere. *Journal of Geophysical Research: Space Physics*, *97*(A2), 1097–1108. https://doi.org/10.1029/91JA01548

Claudepierre, S. G., O'Brien, T. P., Blake, J. B., Fennell, J. F., Roeder, J. L., Clemmons, J. H., et al. (2015). A background correction algorithm for van Allen probes mage is electron flux measurements. *Journal of Geophysical Research: Space Physics*, *120*(7), 5703–5727. https://doi.org/10.1002/2015JA021171

Daggitt, T., Horne, R., Glauert, S., & Del Zanna, G. (2024). Bas-rbm simulations of ultra-relativistic electron acceleration in earth's radiation belts using a coupled plasma density model (version 1.0) [Dataset]. NERC EDS UK Polar Data Centre. https://doi.org/10.5285/ea37228a-5b4d-4db2-8d97-53fff2c43f3f

Glauert, S. A., & Horne, R. B. (2005). Calculation of pitch angle and energy diffusion coefficients with the padie code. *Journal of Geophysical Research: Space Physics*, *110*(A4). https://doi.org/10.1029/2004JA010851

Glauert, S. A., Horne, R. B., & Meredith, N. P. (2014a). Simulating the earth's radiation belts: Internal acceleration and continuous losses to the magnetopause. *Journal of Geophysical Research: Space Physics*, *119*(9), 7444–7463. https://doi.org/10.1002/2014JA020092

Glauert, S. A., Horne, R. B., & Meredith, N. P. (2014b). Three-dimensional electron radiation belt simulations using the bas radiation belt model with new diffusion models for chorus, plasmaspheric hiss, and lightning-generated whistlers. *Journal of Geophysical Research: Space Physics*, *119*(1), 268–289. https://doi.org/10.1002/2013JA019281

Glauert, S. A., Horne, R. B., & Meredith, N. P. (2018). A 30-year simulation of the outer electron radiation belt. *Space Weather*, *16*(10), 1498–1522. https://doi.org/10.1029/2018SW001981

Guo, D., Xiang, Z., Ni, B., Jin, T., Zhou, R., Yi, J., et al. (2023). Three-dimensional simulations of ultra-relativistic electron acceleration during the 21 April 2017 storm. *Journal of Geophysical Research: Space Physics*, *128*(4), e2023JA031407. https://doi.org/10.1029/2023JA031407

Haerendel, G. (1970). On the balance between radial and pitch angle diffusion. In B. M. McCormac (Ed.), *Particles and Fields in the Magnetosphere* (pp. 416–428). Springer Netherlands. https://doi.org/10.1007/978-94-010-3284-1_39

Hartley, D., Christopher, I., Chen, L., Gu, W., Kletzing, C., Santolik, O., et al. (2023). Observations of whistler-mode chorus waves and plasma density variations. In *Conference session*. AGU 2023.

Hartley, D. P., Kletzing, C. A., Chen, L., Horne, R. B., & Santolík, O. (2019). Van Allen probes observations of chorus wave vector orientations: Implications for the chorus-to-hiss mechanism. *Geophysical Research Letters*, *46*(5), 2337–2346. https://doi.org/10.1029/2019GL082111

He, Q., Liu, S., Xiao, F., Gao, Z., Li, T., Shang, X., et al. (2022). Observations and parametric study on the role of plasma density on extremely low-frequency chorus wave generation. *Science China Technological Sciences*, *65*(11), 2649–2657. https://doi.org/10.1007/s11431-021-2030-7

Horne, R. B., Kersten, T., Glauert, S. A., Meredith, N. P., Boscher, D., Sicard-Piet, A., et al. (2013). A new diffusion matrix for whistler mode chorus waves. *Journal of Geophysical Research: Space Physics*, *118*(10), 6302–6318. https://doi.org/10.1002/jgra.50594

Horne, R. B., & Thorne, R. M. (1998). Potential waves for relativistic electron scattering and stochastic acceleration during magnetic storms. *Geophysical Research Letters*, *25*(15), 3011–3014. https://doi.org/10.1029/98GL01002

Horne, R. B., Thorne, R. M., Shprits, Y. Y., Meredith, N. P., Glauert, S. A., Smith, A. J., et al. (2005). Wave acceleration of electrons in the van Allen radiation belts. *Nature*, *437*(7056), 227–230. https://doi.org/10.1038/nature03939

Kersten, T., Horne, R. B., Glauert, S. A., Meredith, N. P., Fraser, B. J., & Grew, R. S. (2014). Electron losses from the radiation belts caused by emic waves. *Journal of Geophysical Research: Space Physics*, *119*(11), 8820–8837. https://doi.org/10.1002/2014JA020366

Kurth, W. S., De Pascuale, S., Faden, J. B., Kletzing, C. A., Hospodarsky, G. B., Thaller, S., & Wygant, J. R. (2015). Electron densities inferred from plasma wave spectra obtained by the waves instrument on van Allen probes. *Journal of Geophysical Research: Space Physics*, *120*(2), 904–914. https://doi.org/10.1002/2014JA020857

LANL. (2012). Emfisis data index [Dataset]. In *EMFISIS Project*. University of Iowa. https://emfisis.physics.uiowa.edu/data/index

LANL. (2013). Rbsp-ect science data products [Dataset]. *RBSP-ECT Science Operations and Data Center*. https://rbsp-ect.newmexicoconsortium.org/science/DataDirectories.php

Liu, W., Tu, W., Li, X., Sarris, T., Khotyaintsev, Y., Fu, H., et al. (2016). On the calculation of electric diffusion coefficient of radiation belt electrons with in situ electric field measurements by Themis. *Geophysical Research Letters*, *43*(3), 1023–1030. https://doi.org/10.1002/2015GL067398

Lyons, L. R., & Thorne, R. M. (1973). Equilibrium structure of radiation belt electrons. *Journal of Geophysical Research (1896-1977)*, *78*(13), 2142–2149. https://doi.org/10.1029/JA078i013p02142

Ma, Q., Li, W., Thorne, R. M., Ni, B., Kletzing, C. A., Kurth, W. S., et al. (2015). Modeling inward diffusion and slow decay of energetic electrons in the earth's outer radiation belt. *Geophysical Research Letters*, *42*(4), 987–995. https://doi.org/10.1002/2014GL062977

Ma, Q., Li, W., Zhang, X.-J., & Bagenal, F. (2020). Energetic electron scattering due to whistler mode chorus waves using realistic magnetic field and density models in Jupiter's magnetosphere. *Journal of Geophysical Research: Space Physics*, *125*(8), e2020JA027968. https://doi.org/10.1029/2020JA027968

Malaspina, D. M., Jaynes, A. N., Elkington, S., Chan, A., Hospodarsky, G., & Wygant, J. (2021). Testing the organization of lower-band whistler-mode chorus wave properties by plasma pause location. *Journal of Geophysical Research: Space Physics*, *126*(1), e2020JA028458. https://doi.org/10.1029/2020JA028458

Mathie, R. A., & Mann, I. R. (2000). A correlation between extended intervals of ulf wave power and storm-time geosynchronous relativistic electron flux enhancements. *Geophysical Research Letters*, *27*(20), 3261–3264. https://doi.org/10.1029/2000GL003822

Matzka, J., Stolle, C., Yamazaki, Y., Bronkalla, O., & Morschhauser, A. (2021). The geomagnetic kp index and derived indices of geomagnetic activity. *Space Weather*, *19*(5), e2020SW002641. https://doi.org/10.1029/2020SW002641

Meredith, N. P., Horne, R. B., Shen, X.-C., Li, W., & Bortnik, J. (2020). Global model of whistler mode chorus in the near-equatorial region (\vert {\lambda}_{m}\vert \lt 18°). *Geophysical Research Letters*, *47*(11), e2020GL087311. https://doi.org/10.1029/2020GL087311

Ross, J. P. J., Glauert, S. A., Horne, R. B., Watt, C., Meredith, N., & Woodfield, E. (2020). A new approach to constructing models of electron diffusion by emic waves in the radiation belts. *Geophysical Research Letters*, *47*(20), e2020GL088976. https://doi.org/10.1029/2020GL088976

Ross, J. P. J., Glauert, S. A., Horne, R. B., Watt, C. E. J., & Meredith, N. P. (2021). On the variability of emic waves and the consequences for the relativistic electron radiation belt population. *Journal of Geophysical Research: Space Physics*, *126*(12), e2021JA029754. https://doi.org/10.1029/2021JA029754

Rostoker, G., Skone, S., & Baker, D. N. (1998). On the origin of relativistic electrons in the magnetosphere associated with some geomagnetic storms. *Geophysical Research Letters*, *25*(19), 3701–3704. https://doi.org/10.1029/98GL02801

Shprits, Y. Y., Allison, H. J., Wang, D., Drozdov, A., Szabo-Roberts, M., Zhelavskaya, I., & Vasile, R. (2022). A new population of ultra-relativistic electrons in the outer radiation zone. *Journal of Geophysical Research: Space Physics*, *127*(5), e2021JA030214. https://doi.org/10.1029/2021JA030214

Subbotin, D. A., & Shprits, Y. Y. (2009). Three-dimensional modeling of the radiation belts using the versatile electron radiation belt (verb) code. *Space Weather*, *7*(10). https://doi.org/10.1029/2008SW000452

Summers, D., & Thorne, R. M. (2003). Relativistic electron pitch-angle scattering by electromagnetic ion cyclotron waves during geomagnetic storms. *Journal of Geophysical Research: Space Physics*, *108*(A4). https://doi.org/10.1029/2002JA009489

Summers, D., Thorne, R. M., & Xiao, F. (1998). Relativistic theory of wave-particle resonant diffusion with application to electron acceleration in the magnetosphere. *Journal of Geophysical Research: Space Physics*, *103*(A9), 20487–20500. https://doi.org/10.1029/98JA01740

Tang, R., Summers, D., & Deng, X. (2014). Effects of cold electron number density variation on whistler-mode wave growth. *Annales Geophysicae*, *32*(7), 889–898. https://doi.org/10.5194/angeo-32-889-2014

Tsyganenko, N., & Sitnov, M. (2005). Modeling the dynamics of the inner magnetosphere during strong geomagnetic storms. *Journal of Geophysical Research*, *110*(A3). https://doi.org/10.1029/2004JA010798

Varotsou, A., Boscher, D., Bourdarie, S., Horne, R. B., Meredith, N. P., Glauert, S. A., & Friedel, R. H. (2008). Three-dimensional test simulations of the outer radiation belt electron dynamics including electron-chorus resonant interactions. *Journal of Geophysical Research*, *113*(A12). https://doi.org/10.1029/2007JA012862

Watt, C. E. J., Allison, H. J., Meredith, N. P., Thompson, R. L., Bentley, S. N., Rae, I. J., et al. (2019). Variability of quasilinear diffusion coefficients for plasmaspheric hiss. *Journal of Geophysical Research: Space Physics*, *124*(11), 8488–8506. https://doi.org/10.1029/2018JA026401

Wong, J.-M., Meredith, N. P., Horne, R. B., Glauert, S. A., & Ross, J. P. J. (2024). New chorus diffusion coefficients for radiation belt modeling. *Journal of Geophysical Research: Space Physics*, *129*(1), e2023JA031607. https://doi.org/10.1029/2023JA031607

Woodfield, E. E., Glauert, S. A., Menietti, J. D., Averkamp, T. F., Horne, R. B., & Shprits, Y. Y. (2019). Rapid electron acceleration in low-density regions of Saturn's radiation belt by whistler mode chorus waves. *Geophysical Research Letters*, *46*(13), 7191–7198. https://doi.org/10.1029/2019GL083071

Zhao, H., Baker, D., Li, X., Malaspina, D., Jaynes, A., & Kanekal, S. (2019). On the acceleration mechanism of ultrarelativistic electrons in the center of the outer radiation belt: A statistical study. *Journal of Geophysical Research: Space Physics*, *124*(11), 8590–8599. https://doi.org/10.1029/2019JA027111